RSC Advances

This article can be cited before page numbers have been issued, to do this please use: M. Akter, S. S. Satter, A. K. Singh, M. M. Rahman, M. Y. A. Mollah and Md. A. B. H. Susan, *RSC Adv.*, 2016, DOI: 10.1039/C6RA14955C.

RSC Advances

View Article Online
DOI: 10.1039/C6RA14955C

Hydrophilic ionic liquid-assisted control of size and morphology of ZnO nanoparticles prepared by chemical precipitation method

Mousumi Akter,[a] Shazia Sharmin Satter,[a] Ajaya Kumar Singh,[b] M. Muhibur Rahman,[c] M. Yousuf A. Mollah[c] and Md. Abu Bin Hasan Susan[a]*

[a]*Department of Chemistry, University of Dhaka, Dhaka 1000, Bangladesh*

[b]*Department of Chemistry, Govt. V. Y. T. PG. Autonomous College, Chhattisagarh, India*

[c]*University Grants Commission of Bangladesh, 29/1 Agargaon, Sher-E-Bangla Nagar, Dhaka 1207, Bangladesh*

AUTHOR EMAIL ADDRESS: susan@du.ac.bd

CORRESPONDING AUTHOR FOOTNOTE: To whom correspondence should be addressed. Telephone/Fax: 88029661920 Ext. 7162; Fax: +88 029667222
E-mail: susan@du.ac.bd (M. A. B. H. Susan)

View Article Online
DOI: 10.1039/C6RA14955C

ABSTRACT

ZnO nanoparticles (NPs) were prepared by chemical precipitation method from zinc acetate dihydrate and NaOH using isopropanol as the reaction medium. The influence of an imidazolium-based hydrophilic ionic liquid (IL), 1-ethyl-3-methylimidazolium methylsulfate, [EMIM][$MeSO_4$] at different concenrations on the size and morpholgy of ZnO NPs was investigated. The NPs were characterized by Fourier transform-infrared, energy dispersive X-ray and UV-visible spectroscopy, along with x-ray diffraction, particle size analysis, field emission scanning electron microscopy and high resolution transmission electron microscopy. Pure nanocrystalline ZnO with hexagonal wurtzite phase was formed in the system. The particle size of the NPs varied in the range of 2-55 nm depending on the concentration of the IL used during preparation. With increasing concentration of [EMIM][$MeSO_4$] the shape of the NPs also changed interestingly from spheres to flakes through nanorods. The use of the IL has been proved effective as a self directing agent and templating material for the successful preparation of ZnO nanostructures. Finally, the mechanism for preparation of ZnO NPs with controllable size and morphlogy has been established and the variation of size, shape and morphology has been explained in terms of hydrogen bonding -co- π-π* stacking interaction between IL and the NPs.

View Article Online
DOI: 10.1039/C6RA14955C

1. Introduction

Metal oxide nanoparticles (NPs), due to their exclusive physicochemical properties originated from quantum size effect and single electron transitions, have been the most intriguing materials in recent years.[1] Among the nanostructured materials of this variety, ZnO NPs have been the most promising one for their flexible uses in an assortment of fields. [2-8] ZnO is a semiconductor with wide band gap (~3.37 eV) with large free exciton binding energy (~60 MeV).[9-12] ZnO NPs have been found promising for short-wavelength optoelectronic applications, as efficient adsorbent for removal of various toxic and hazardous chemicals and dyes,[13-16] in magnetic devices where well-defined magnetization axes and switching fields are required to store or to process information, and [16-18] for antibacterial applications.[19-20]

The properties of the ZnO NPs may be tuned widely by varying their size and morphology. Przybyszewska *et al.* used ZnO with different surface areas, particle sizes and morphologies (spheres, whiskers, snowflakes) as cross linking agents of carboxylated nitrile elastomer and determined the relationship between the characteristics of ZnO and its activity in the cross linking process.[21] ZnO nanorod arrays grown onto a fibrous substrate by a low-temperature growth technique were reported to provide excellent UV protection.[22] Ates *et al.* synthesized ZnO nanowires which impart self-cleaning, superhydrophobicity and UV blocking properties.[23] Ma *et al.* demonstrated superior photocatalytic performance of ZnO nanorods and nanoflowers compared to commercial ZnO particles on methyl orange.[24] Besides organic dyes, UV-induced photocatalytic degradation of stearic acid by ZnO nanowires was also reported.[25] Chaudhary *et al* used eight different dyes to check the removal performance of 1-butyl-3-methylimidazoliumtetrafluoroborate[BMIM][BF_4]-functionalized ZnO NPs and established that ZnO NPs are promising nanoadsorbents, which can be efficiently used for treatment of waste water effluents.[26]

Major nanostructures so far realized are nano-spheres, nano-wires, nano-rods, tetrapods, nano-belts, nano-plates, nano-flowers, nano-tubes, nano-pyramids, nano-particles, quantum dots, etc.[27-34] These involve methods using high temperature or prolonged duration, such as, thermal decomposition,[35-36] sol-gel,[37-38] hydrothermal,[39-40] microemulsion,[41] chemical vapour deposition,[42] electrochemical-thermal[43-44] and precipitation techniques[45]. It is therefore desirable to esablish a methodology avoiding the use of expensive raw materials and complicated equipments. However, preparation of ZnO NPs with tunable size and

View Article Online
DOI: 10.1039/C6RA14955C

morphology using a convenient and facile way for large-scale production still remains a challenging task.

Research to-date includes numerous attempts to fabricate ZnO nanostructures using different capping agents such as, poly(vinyl alcohol), poly(vinyl pyrrolidone), starch, ligands, and molecular solvents.[46-47] On the other hand, there are only few reports on the use of ionic liquids (ILs) as a medium or additive for preparation of ZnO NPs with controlled dimension and morphology.[48-59] ILs are composed entirely of ions and possess unique physicochemical properties which inter alia, include: low melting point, negligible vapor pressure, high thermal stability, recyclability and high ionic conductivity. In analogy to solvent templates, ILs with special cations and anions can be appropriately tailored to obtain several special functions and accordingly ILs can serve as solvent stabilizer, template and so on. In fact, the unique structures and properties of ILs can provide ZnO nanomaterials with special morphologies, novel structures, and improved properties and these may be tuned by varying concentration of the IL.

ILs are known as designer salts and hydrophilicity or hydrophobicity of ILs can be fine-tuned by simply varying the cationic or anionic parts of the IL. Interestingly, the works reported so far aims at establishment of the mechanism based on the influence of hydrophobic ILs on the morphology and size of ZnO nanomaterials.[60-63] X. Duan *et al* reported ILs as highly efficient media for preparation of different types of metal oxides.[64] Rabieh and Bagheri synthesized nanosized ZnO based on the reaction of zinc acetate and NaOH in 1-butyl-3-methylimidazolium chloride [BMIM]Cl under ultrasonic irradiation.[60] Oprea *et al* prepared ZnO NPs in mixtures of ILs based on imidazolium cation with organic solvents by a simple one-step solution route at low temperature where shapes of ZnO were spherical and polyhedral.[61] Qi *et al* prepared ZnO rings with controllable morphology in presence of 1-propyl-3-methylimidazolium bromide, [PrMIM][Br] and morphology changed from ring to tube shape with change in concentration of the IL.[62] He and Alexandridis discussed the stability of NP dispersions in ILs and reported that the organization of NPs in ILs is affected by intermolecular interactions, along with other forms of IL and NP hybrids and their applications.[63]

Development of a methodology using hydrophilic ILs to tune size and morphology of metallic NPs, in particular, ZnO NPs on the other hand is still in the rudimentary stage. Recently, Wittmar *et al* synthesized ZnO nanostructures in presence of three different

View Article Online
DOI: 10.1039/C6RA14955C

hydrophilic ILs, 1-ethyl-3-methylimidazolium tetrafloroborate ([EMIM][BF_4]), 1-butyl-3-methylimidazolium tetrafloroborate ([BMIM][BF_4]) and 1-hexyl-3-methylimidazolium tetrafloroborate ([HMIM][BF_4]).[65] Gandhi *et al* reported highly co-ordinating and weaker hydrogen bonding strength for the anion, PF_6^- of a hydrophobic IL, [BMIM] [PF_6^-] and explained that the interaction between the formed nuclei and the anion is too weak to serve effectively for nucleation and growth as compared to hydrophilic ILs.[66] Systematic study by varying concentration of a hydrophobic IL is crucial to understand the mechanism for change in size and morphology of ZnO NPs and ensure tunability. Furthermore, the use of chemical precipitation method is desirable for large-scale production of ZnO since it is simple, cost-effective, environmentally benign, and reliable. However, the route has not yet been attempted using ILs for facile synthesis of ZnO NPs.

In this study, we prepared ZnO NPs, for the first time, using chemical precipitation method in the presence of a hydrophilic IL, 1-ethyl-3-methylimidazolium methylsulfate, [EMIM][$MeSO_4$] and examined the influence of the IL of varying concentrations on the size and morphology of ZnO NPs. Attempt has finally been made to unveil the role of the IL to control the size and morphology of the nanostructure of ZnO.

2. Experimental

2.1 Materials

Zinc acetate dihydrate ($Zn(OAc)_2.2H_2O$, >98%; Merck), sodium hydroxide (NaOH, >98%; Merck) and isopropanol ($(CH_3)_2CHOH$, >99.5%; Fisher Scientific) were used as received. [EMIM][$MeSO_4$] was dried under vacuum at 100 ^oC prior to use (>98%; Sigma Aldrich).

2.2 Method of preparation

0.1 mmol of $Zn(OAc)_2.2H_2O$ was dissolved in 5.0 mL of isopropanol under vigorous stirring at 50 ^oC and subsequently diluted with isopropanol to a total volume of 9.2 mL. [EMIM][$MeSO_4$] was added to the $Zn(OAc)_2$ solution at a volume required to achieve a desired concenration in the range of 0.1-5.0% (v/v). A stock slution of 0.02 M sodium hydroxide solution was prepared in isopropanol. 0.8 mL of freshly prepared NaOH solution was then slowly added to the solution in a beaker at 0 ^oC under constant stirring. The beaker was then immersed in a thermostated water bath at the growth temperature (50 ^oC) for up to 2 hr allow the growth of ZnO.

View Article Online
DOI: 10.1039/C6RA14955C

2.3 Characterization

An Fourier transform-infrared/near infrared (FT-IR/NIR) spectrometer (Frontier FT-IR/NIR, PerkinElmer, USA) was used for molecular characterization of the compounds. FT-IR spectrum was recorded by mixing small amount of solid sample of NPs with KBr to make pellets. The spectrum was recorded in the wavenumber range of 4000-400 cm^{-1}.

X-ray diffraction patterns of the prepared ZnO NPs in absence of IL were recorded by Philips PW-1724 with XDC-700 Guinier Hagg focusing camera using Cu Kα radiation (λ=1.540598Å). The phase composition was analyzed with a wide range of Bragg angles; 2θ ranging from 0 to 90° to determine crystalline structure and crystallite size of ZnO NPs. X-ray was exposed for 15 min on an image plate for each sample. Image plate was scanned using HD-CR 35 NDT/ CR 35 NDT scanner to get intensity vs. line position in mm, which was then converted to intensity vs. 2θ to get the complete diffraction pattern.

Spectroscopic measurements were carried out using a Spectro UV-visible double beam spectrophotometer (model, Labmed UVD-500). The absorption spectra of ZnO NPs synthesized in absence and in presence of IL were recorded using isopropanol or isopropanol with desired concentration of IL as the reference.

The hydrodynamic diameter (D_h) of ZnO NPs was measured by using Zeta sizer Nano ZS90 (ZEN3690, Malvern instruments Ltd, UK) by dynamic light scattering technique. A He-Ne laser beam of 632.8 nm wavelength was used and the measurements were made at a fixed scattering angle of 90°. Isopropanol was used as a dispersant and the dispersions were sonicated prior to measurement. A measuring glass cell of 10 mm diameter was used. The accuracy of the D_h determined by DLS measurements was approximately ±2%.

Morphological analyses of ZnO NP samples were performed using JEOL analytical field emission scanning electron microscope (FESEM, model: JSM-7600F), analytical scanning electron microscope (SEM, model JSM-6490LA) and high resolution transmission electron microscope (HRTEM, model: JEOL JEM 2100 HRTEM). To perform FESEM analysis, samples were mounted on a carbon tape which was attached on a round-shaped sample stage of copper. A drop of NPs in isopropanol was poured on the carbon tape attached with the copper stub and images were taken at an accelerating voltage of 5 KV with magnifications ranging from 10000-130000. For analytical SEM, samples were taken on carbon coated aluminum stubs followed by sputter coating a thin layer of platinum for the measurements at an acceleration voltage of 20 kV. Elemental analysis of the sample was carried out in an energy-dispersive X-ray (EDX) spectrometer attached with FESEM JEOL

View Article Online
DOI: 10.1039/C6RA14955C

7600F. Sample stages of copper with conducting carbon tape were used throughout the investigation. The EDX spectrum was taken by selecting several spots or zone of a specific particle of the sample. The accelerating voltage was 10 keV and counting rate was varied from 1376-3343 cps. To perform HRTEM analysis, ZnO nanostructures were dispersed into isopropanol and sonicated for 30 min; a drop of this solution was used to make a thin layer on copper coated grid and allowed to dry. Micrographs were taken at different magnifications at 200 kV. Length of the camera was 499.606 mm with a resolution of 0.24 nm**.** Selected area electron diffraction (SAED) pattern of NPs were also analyzed along with HRTEM.

3. Results and discussion

FT-IR spectrum of ZnO NPs in isopropanol (Fig. 1) shows stretching vibration of Zn-O band at 456 cm^{-1} to confirm the presence of ZnO. The stretching asymmetric vibrations of >C=O bond is observed at 1454 cm^{-1} due to the presence of residual $Zn(OAc)_2$ in the reaction media. FT-IR spectrum of ZnO NPs in isopropanol in presence of the IL shows stretching vibration of Zn-O bond at 450 cm^{-1}. The strong absorption peak in the range of 1050-1217 cm^{-1} is observed due to the stretching mode of vibration in the >C-N bond. The absorption band at 1645 cm^{-1} corresponds to the stretching vibration of >C=N bond in the sample.

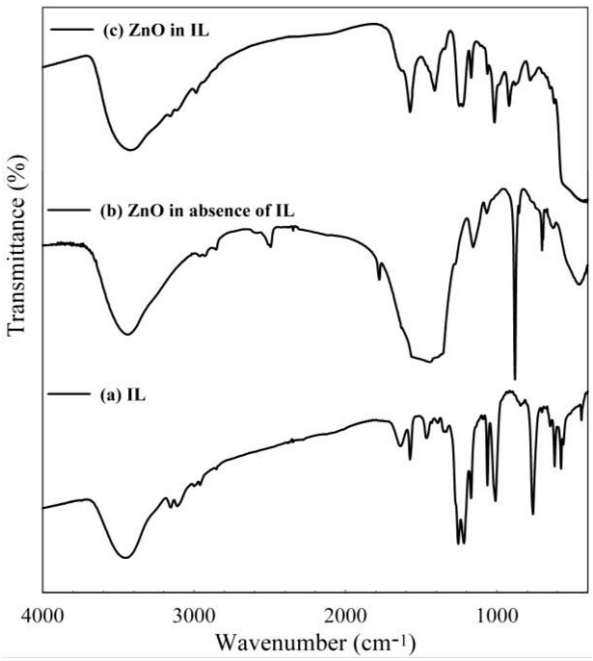

Fig. 1 FT-IR spectrum of (a) the IL, [EMIM][$MeSO_4$], (b) ZnO NPs, and (c) ZnO NPs in [EMIM][$MeSO_4$].

View Article Online
DOI: 10.1039/C6RA14955C

The EDX spectrum of ZnO NPs confirms the presence of the elements Zn and O. In addition to an oxygen peak at 0.6 keV, signals corresponding to Zn at about 1.01, 8.7 and 9.5 keV were observed, which is indicative of successful preparation of ZnO NPs. (Fig. S1 ESI†).

All the lines in the x-ray powder diffraction pattern of ZnO NPs in absence of IL (Fig. 2) are perfectly indexed as hexagonal cubic packed. The diffraction peaks appearing at 31.5°, 34.6°, 36.4°, 47.5°, 56.7° and 66.1° correspond to the miller lattice indices of (100), (002), (101), (102), (110), and (200), respectively. This XRD pattern confirmed the wurtzite structure of ZnO NPs in absence of IL. A definite line broadening of the XRD peaks indicates that the prepared material consist of particles in nanoscale range. The experimental *d*-values are in good agreement with the Joint Committee on Powder Diffraction Standards (JCPDS) *d*-values (JCPDS Card No. 36-1451).[67] The lines for prepared ZnO NPs in absence of IL are very intense showing a higher degree of crystallinity.

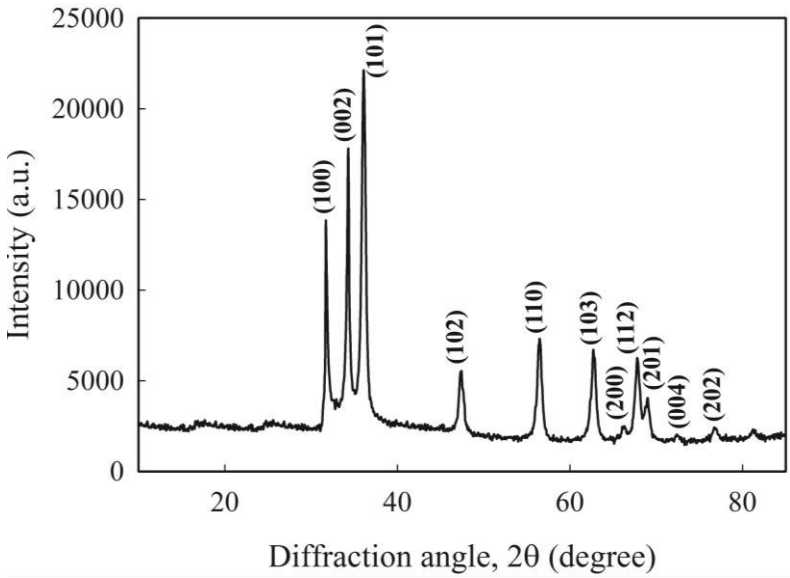

Fig. 2 X-Ray diffraction pattern of ZnO NPs in absence of IL.

The synthesized ZnO NPs, both in presence and absence of the IL shows strong absorption band in the UV-region. In absence of [EMIM][$MeSO_4$], the absorption peak centred at lower wavelength (wavelength corresponding to absorption maximum, $\lambda_{max} \approx 334$ nm); but in presence of 0.1% [EMIM][$MeSO_4$] the absorption peak shifts to slightly higher wavelength ($\lambda_{max} \approx 340$ nm) (Fig. 3). The absorption peak shifted to

higher wavelength with further increase in the concentration of the IL (e.g. for 1% [EMIM][$MeSO_4$] $\lambda_{max} \approx 356$ nm). The bathochromic shift in the characteristic peak with increase in concentration of the IL indicates that particle size increases with increase in concentration of the IL in the reaction media. However, when the concentration of the IL was very high, no such characteristic peak could be identified for ZnO NPs (Figure not shown).

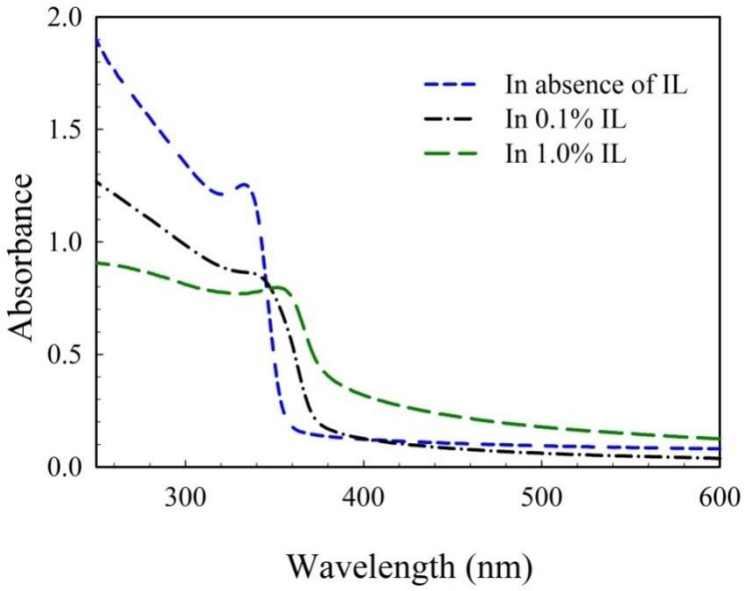

Fig. 3 Absorption spectra of ZnO NPs in isopropanol (a) without [EMIM][$MeSO_4$], (b) with 0.1% [EMIM][$MeSO_4$], and (c) with 1.0% [EMIM][$MeSO_4$].

Distributions of particle size of ZnO NPs prepared using [EMIM][$MeSO_4$] in isopropanol in the concentration range of 0.1 to 5.0% (*v*/*v*) are shown in Fig. 4**.** The D_h of the NPs distributed in isopropanol showed interesting variations.

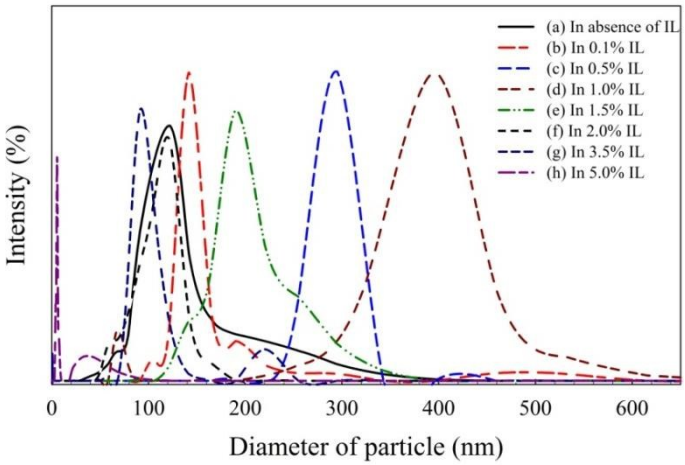

Fig. 4 Particle size distribution of ZnO NPs prepared at different concentrations of [EMIM][$MeSO_4$].

View Article Online
DOI: 10.1039/C6RA14955C

The d_h of ZnO NPs in isopropanol increased with increasing concentration of [EMIM][$MeSO_4$] and decreased most at 5% IL. Variation of the Z-average diameter of ZnO NPs with concentration of the IL is shown in Fig 5. The Z-average diameter of ZnO NPs prepared from 0.5% of IL in isopropanol is 158 nm, which is higher than the ZnO nanostructure produced in presence of 0.1% IL (around 130 nm). The Z-average particle size ZnO NPs produced in presence of 1.0% IL had a maximum value of 261 nm. The mean diameter of ZnO NPs prepared from 5% of the IL is only 40 nm, which is the smallest compared to NPs prepared from other concentrations of the IL.

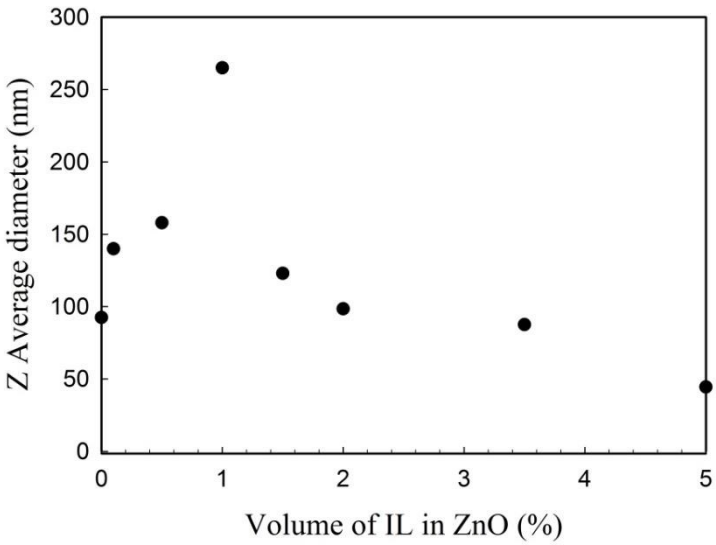

Fig. 5 Variation of Z-average diameter of ZnO NPs with concentration of [EMIM][$MeSO_4$].

The size of the products depends on the rate of nucleation and the growth rate of the product. Addition of small concentration of [EMIM][$MeSO_4$] to the reaction medium cannot resist the growth of ZnO NPs to a larger extent. The growth rate may be higher than the nucleation rate to result in larger particle size. The IL may act as a template to induce the privileged growth of ZnO crystal nuclei to a certain direction, thus allowing the nanocrystals to undergo self-organization into the desired nanostructure.

The IL may serve as an agglomeration inhibitor at higher concentrations, which can hinder the fast contact of particles of two substrates. The reaction is slightly slower but allows the molecules to self-assemble and the rate of nucleation is faster than the growth rate. The unique structure of the [EMIM][$MeSO_4$] may also induce the preferential growth of ZnO crystal nuclei in a certain direction, thus allowing the

View Article Online
DOI: 10.1039/C6RA14955C

nanocrystals to undergo self-organization into the desired nanostructure, just as a soft template.

FESEM images were used for the morphological analysis of ZnO NPs prepared at different concentrations of [EMIM][$MeSO_4$]. Fig. 6 shows FESEM images of ZnO NPs prepared in the absence and in presence of the IL at different concentrations. The morphology of ZnO in absence of [EMIM][$MeSO_4$] exhibits well-defined ZnO nanostructures composed of nanosized, regular, and uniform spherical particles [Fig 6a]. ZnO NPs prepared using 0.1% (*v*/*v*) [EMIM][$MeSO_4$] comprise both spherical and capsular NPs with prominent agglomeration (Fig. 6b). ZnO NPs from 0.5% (v/v) [EMIM][$MeSO_4$] exhibit a variety of morphologies and irregular shapes, such as deformed sphere, capsule, and elongated rods with sharp edges (Fig 6c). The ZnO NPs prepared using 1% (*v*/*v*) [EMIM][$MeSO_4$] on the other hand, are like flakes (Fig 6d). Agglomeration is noted for ZnO NPs prepared from 1.5% (*v*/*v*) [EMIM][$MeSO_4$] to yield a mixture of spherical and capsule-shaped particles. With further increase in concentration of the IL, (2%, 3% and 5% (v/v) [EMIM][$MeSO_4$), ZnO NPs become spherical and the size becomes minimum at 5% (*v*/*v*) [EMIM][$MeSO_4$].

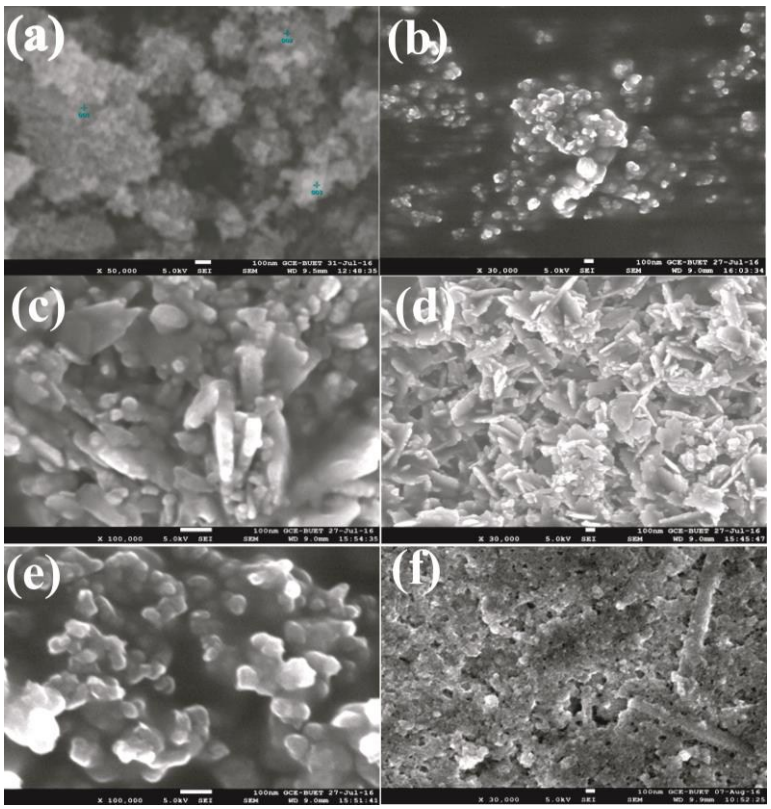

Fig. 6 FESEM images of ZnO NPs in (a) in absence of [EMIM][$MeSO_4$] and in presence of (b) 0.1% (c) 0.5% (d) 1% (e) 1.5% (f) 5.0% [EMIM][$MeSO_4$].

View Article Online
DOI: 10.1039/C6RA14955C

Fig. 7 shows the HRTEM images of ZnO NPs. The morphologies of ZnO NPs observed from TEM images are consistent with the FESEM images (Fig. 6). Size distribution histograms from HRTEM images (Insets of Fig 7) show that the diameters of ZnO nanostructures prepared from of 0.1%, 1.0% and 5.0% (*v*/*v*) [EMIM][$MeSO_4$] are below 17 nm; while the the diameter for that from 0.5% [EMIM][$MeSO_4$] ranged from 15-55 nm. The crystallinity of ZnO NPs could also be judged from the selected area diffraction pattern (SAED) of the HRTEM images at higher magnifications for ZnO NPs (Fig. 8). SAED patterns provide clear evidence that ZnO NPs are polycrystalline in agreement with XRD results. The diffraction rings on SAED image match with the peaks in XRD pattern of ZnO NPs to infer hexagonal wurtzite structure for ZnO NPs.[68] The HRTEM images (part b and c of Fig. 8) of ZnO NPs prepared from 0.5% and 1.0% (*v*/*v*) shows the interplanar spacing to be around 0.5 nm. This is close to the separation between the adjacent two (0001) lattice planes of hexagonal ZnO to indicate that the ZnO nanostructures exhibit a preferred growth orientation along the [0001] crystal axis.[69]

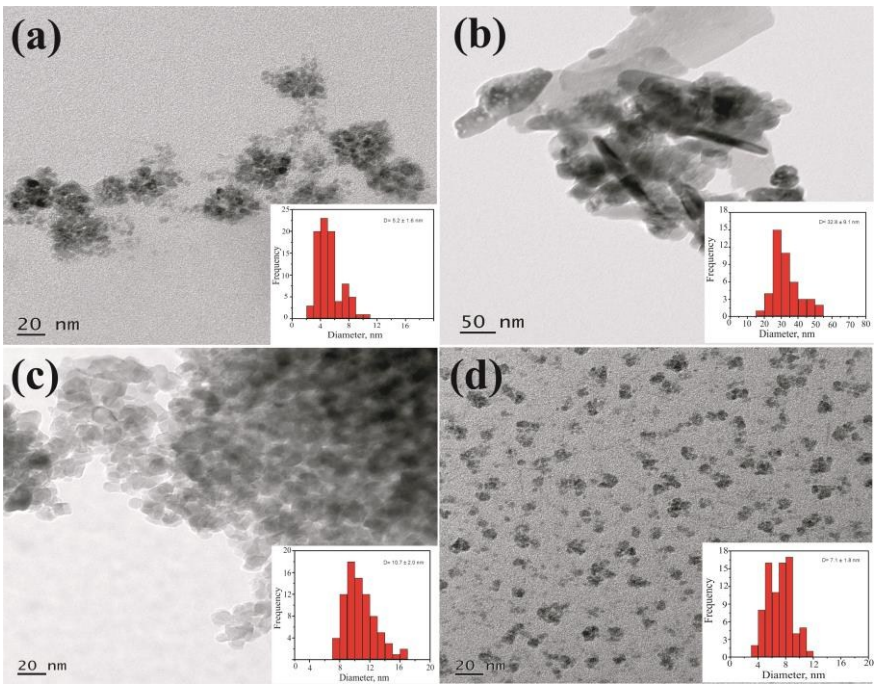

Fig. 7 HRTEM images of ZnO NPs prepared from (a) 0.1% (c) 0.5% (d) 1% (e) 5.0% [EMIM][$MeSO_4$] in isopropanol. Inset shows the size distribution.

View Article Online
DOI: 10.1039/C6RA14955C

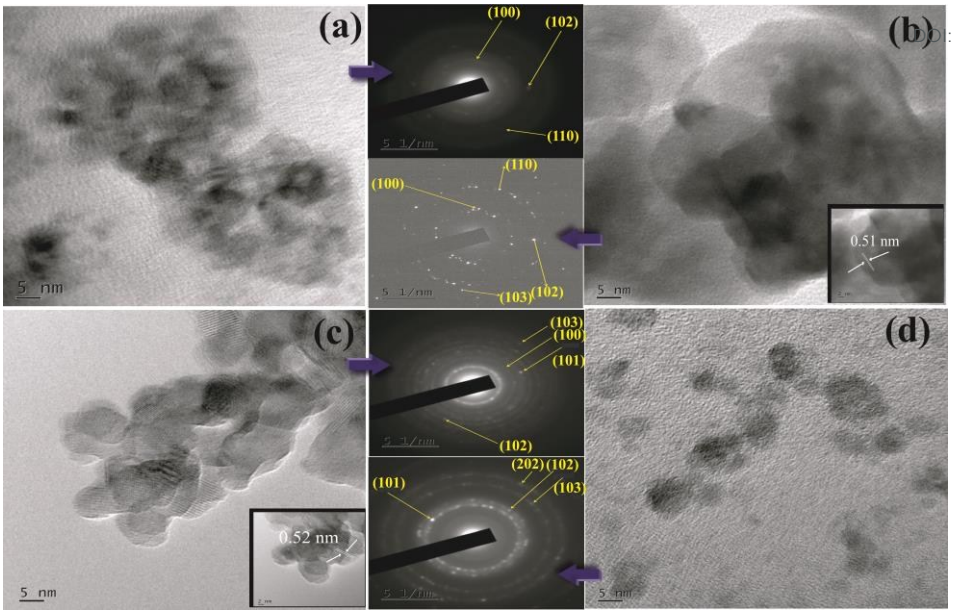

Fig. 8 Selected area diffraction pattern of HRTEM images at higher magnifications of ZnO NPs prepared from (a) 0.1% (c) 0.5% (d) 1% (e) 5.0% [EMIM][$MeSO_4$].

ZnO nanostructures with appealing morphologies such as spheres, nanorods and nanocapsules, nanoflakes were obtained for different concentrations of hydrophilic IL, [EMIM] [$MeSO_4$]. The mechanism may be established based on experimental results and literature. The growth unit for ZnO crystal is in general considered to be $Zn(OH)_4^{2-}$.[70]

$$Zn(OAc)_2.2H_2O + NaOH = Zn(OH)_2 + 2CH_3COONa + 2H_2O$$

$$Zn(OH)_2 + 2H_2O = Zn(OH)_4^{2-} + 2H^+$$

$$Zn(OH)_4^{2-} \xrightarrow[\text{2 hr}]{\text{Magnetic stirring}} ZnO + H_2O + 2OH^-$$

[EMIM] [$MeSO_4$] acts as a size and shape directing agent. The remarkable influence on the shapes and structures of the ZnO nanostrusctures prepared from IL relies on hydrogen bonding, π-π*stacking interactions, self-assembly, electrostatic attraction, and so on.[71-72]

When [EMIM][$MeSO_4$] is added at low concentrations to the reaction medium, the IL may dissociate into constituent ions. The cation, $[EMIM]^+$ may interact with the bulk because of its electron withdrawing ability by sharing of electron pair of hydrogen and carbon at position 2 of the imidazole ring (Fig. 9). [EMIM][$MeSO_4$] is adsorbed on the surface of the growing ZnO crystals, restricting growth of the forming material to some extent. This causes

View Article Online
DOI: 10.1039/C6RA14955C

anisotropic growth of the crystal. Thus it is reasonable that the IL promotes the formation of different nanostructures through hydrogen bonding-co-π-π* stacking mechanism.

When IL is added at high concentrations to the reaction media, then ion clusters may be formed.[73] Positively or negatively charged ion clusters, instead of separating into single ions, may surround the NP surface to build an electrical double-layer, thus providing an electrostatic force to keep the NPs apart from each other.[63] Here, the nucleation rate may be higher than the growth rate. Therefore, the resulting morphology of ZnO nanostructure is spherical.

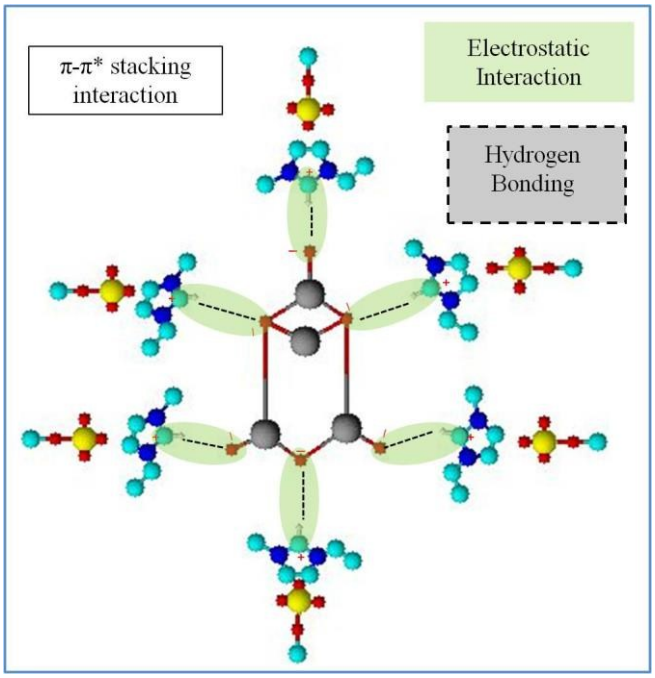

Fig. 9 Schematic representation of interaction between [EMIM][$MeSO_4$] and ZnO crystal.

The shape of ZnO nanostructures varies with increasing concentration of IL. The cations of the IL are attracted to the surface of negative charged NPs to form a positive ion layer, and then counter ions form a second layer on the surface of the NPs by electrostatic attraction. Thus, it is the difference in the interaction between the IL and the growing ZnO nuclei which gives rise to different shapes from capsule to spheres in nanodimension. The mechanism is shown schematically in Fig. 10.

View Article Online
DOI: 10.1039/C6RA14955C

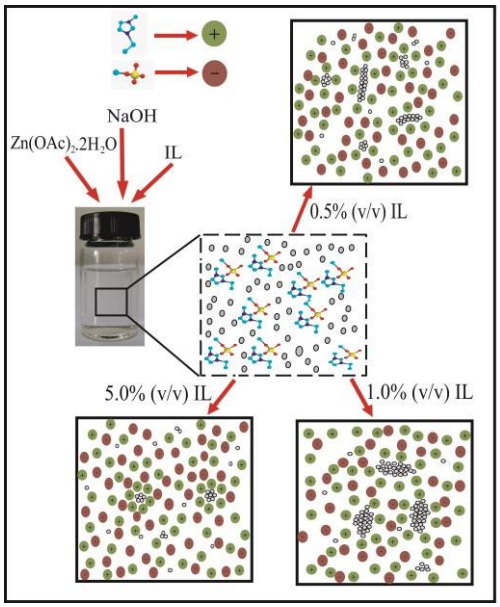

Fig. 10 Schematic representation of different morphology formed by the interaction of ZnO and [EMIM][$MeSO_4$].

It may be worth mentioning that we used a single precursor salt concentration (0.01 M of $Zn(OAc)_2.2H_2O$) and varied IL concentration for this study. The concentration of $Zn(OAc)_2.2H_2O$ is likely to have a great impact on the size and morphology of the prepared ZnO NPs. With increasing concentration of zinc acetate in the system the growth rate has been reported to be more than the nucleation rate.[74-75] The particle size is likely to be larger. It would be interesting to study the role of precursor salt concentration of the size and morphology through extensive studies using different ILs and we shall publish it elsewhere.

4. Conclusions

ZnO nanostructures with distinct morphologies and controllable size have been successfully prepared by chemical precipitation method in presence of [EMIM][$MeSO_4$] at different concentrations. ZnO NPs prepared have structures in nanodimensions like sphere, capsule, flakes and rod depending on the concentrations of the IL. The particle size of the NPs varied interestingly depending on the concentration of the IL used during preparation. The use of a hydrophilic IL has been proved effective as a self directing agent and templating material for the successful synthesis of ZnO nanostructures and systematic variation of the concentration of [EMIM][$MeSO_4$] results in variation in size and morpholgy of ZnO NPs. A higher concentration of the IL lowers the size of spherical ZnO NPs.

View Article Online
DOI: 10.1039/C6RA14955C

Acknowledgements

The authors acknowledge the use of laboratory equipment for the present work procured under subproject CP 231 of the Higher Education Quality Enhancement Project of the Ministry of Education, Government of Bangladesh. The authors also express their gratitude to the Centre for Advanced Research in Sciences of Dhaka University, Bangladesh for permitting the use of SEM, Multi Scale Characterization Lab of the Department of Glass and Ceramic Engineering of BUET for FESEM and EDX and the Sophisticated Test and Instrumentation Centre, Kochi University, India for HRTEM facilities.

View Article Online
DOI: 10.1039/C6RA14955C

Notes and references

1 G. Oskam, *J. Sol-Gel Sci. Technol.*, 2006, **37**, 161–164.

2 G. Xiong, U. Pal, J. G. Serrano, K. B. Ucer and R. T. Williams, *Phys. Stat. Sol.*, 2006, 3577–3581

3 M. I. Khalil, M. M. Al-Qunaibit, A. M. Al-Zahem and J. P. Labis, *Arab. J. Chem*., 2014, **7**, 1178-1184.

4 G. C. Yi, C. Wang and W. Park, *Sem. Sci. Tech.*, 2005, **20**, 22-34.

5 W. J. E. Beek, M. M. Wienk and R. A. J. Janssen, *Adv. Mater*, 2004, **16**, 1009-1013.

6 S. Sultana, M. S. Miran, M. Y. A. Mollah, M. M. Rahman, *J. Bangladesh Chem. Soc.*, 2008, **21**, 29.

7 P. Ahmed, M. S. Miran, M. A. B. H. Susan, M. Y. A. Mollah, *J. Bangladesh Chem. Soc.*, 2013, **26**, 60.

8 S S. Satter, M. Hoque, M. M. Rahman, M. Y. A. Mollah and M. A. B. H. Susan, *RSC Adv*., 2014, **4**, 20612.

9 D G Thomas, *J. Phys. Chem. Solids*, 1960, **15,** 86.

10 M. Dvorak, S. Wei, and Z. Wu, *Phys. Rev. Lett*., 2013, **110**, 016402.

11 Y. Q. Su, Y. Zhu, D. Yong, M. Chen, L. Su, A. Chen, Y. Wu, B. Pan and Z. Tang, *J. Phys. Chem. Lett.*, 2016, **7**, 1484–1489.

12 B. Subash, B. Krishnakumar, M. Swaminathan and M. Shanthi, *Ind. Eng. Chem. Res*., 2014, **53**, 12953–12963.

13 C. Mondal, J. Pal, M. Ganguly, A.K. Sinha, J. Jana and T. Pal, *New J. Chem*., 2014, 38, 2999–3005.

14 K. K. Chattopadhyay, S. Maiti and S. Pal, *Cryst. Eng. Comm.*, 2015, **17**, 9264-9295.

15 E. Kowsari and B. Bazri, *Appl. Catal A*, 2014, **475**, 325–334.

16 J. M. Hancock, W. M. Rankin, T. M. Hammad, J. S. Salem, K Chesnel and R. G. Harrison, *J. Nanosci. Nanotechnol.*, 2015, **15**, 3809-15.

17 M. A. Garcia, J. M. Merino, E. F. Pinel, A. Quesada, J. de la Venta, M. L. R. González, G. R. Castro, P. Crespo, J. Llopis, J. M. González-Calbet, and A. Hernando, *Nano Lett.*, 2007, **7**, 1489–1494.

18 H. Xu, Q. Zhao, H. Yang and Y. Chn, J. Nanopart. Res., 2009, **11**, 615.

19 A. Sirelkhatim, S. Mahmud, A Seeni, N. H. M. Kaus, L. C. Ann, S. Khadijah, M.

Bakhori, H. Hasan and D. Mohamad, *Nano-Micro Lett*., 2015, 7, 3, 219–242.

20 K. R. Raghupathi, R. T. Koodali, and A. C Manna, *Langmuir*, 2011, 27, 4020–4028.

21 M. Przybyszewska and M. Zaborski, *Express Polym. Lett*., 2009, **3**, 542–552.

22 R. Wang, J. H. Xin, X. M. Tao and W. A. Daoud, *Chem. Phys. Lett*., 2004, **398**, 250–255.

23 E. S. Ates and H. E. Unalan, *Thin Solid Films*, 2012, **520**, 4658–4661.

24 S. S. Ma, R. Li, C. P. Lv, W. Xu and X. L Gou, *J. Hazard. Mater*. 2010, **192**, 730–740.

25 G. Kenanakis and N. Katsarakis, *Appl. Catal. A Gen*., 2011, **378**, 227–233.

26 S. Chaudhary, Y. Kaur, A. Umar and G. R. Chaudhary, *J. Mol. Liq*.,2016, **220**, 1013–1021

27 P. Gao, J. Lee and Z. Wang, *J. Phys. Chem. C*, 2007, 13763–13769.

28 B. Liu and H. Zeng, *J. Am. Chem. Soc*., 2003, **125**, 4430–4431.

29 Z. Li, Y. Xiong and Y. Xie, *Inorg. Chem*., 2003, **42**, 8105–8109.

30 J. Xie, P. Li, Y. Wang and Y. Wei, *J. Phys. Chem. Solids*, 2009, **70**, 112–116.

31 A. Wei, X. Sun and C. Xu, *Nanotechnol*., 2006, **17**, 1740–1744.

32 Z. Gui, J. Liu, Z. Wang; *J. Phys. Chem. B*; 2005, **109**, 1113–1117

33 Y. H. Ni, X. W. Wei, X. Ma and J. M. Hong, *J. Cryst. Growth*, 2005, **283**, 48–56.

34 H. Zhao, X. Su, F. Xiao, J. Wang and J. Jian, *Mat. Sci. Eng*. B, 2011, **176**, 611–615.

35 S. Baskoutas, P. Giabouranis, S. N. Yannopoulos, V. Dracopoulos, L. Toth, A. Chrissanthopoulos and N. Bouropoulos, *Thin Solid Films*, 2007, **515**, 8461–8464.

36 B. Hutera, A. Kmita, E. Olejnik and T. Tokarski, *Metall. Mater*., 2011, **58**, 489–491.

37 M. Ristiac, S. Musiac, M. Ivanda and S. Popoviac, *J. Alloys Compd*., 2005, **397**, 1-4.

38 H. Y. Yue, W. D. Fei, Z. J. Li and L. D. Wang, *J. Sol-Gel Sci. Technol*., 2007, **44**, 259–262.

39 H. Zhang, D. Yang, Y. Ji, X. Y. Ma, J. Xu and D. L. Que, *J. Phys. Chem. B*,

View Article Online
DOI: 10.1039/C6RA14955C

2004, **18**, 3955–3958.

40 D. Ramimoghadam, M. Z. B. Hussein and Y. H. Taufiq-Yap, *J. Phys. Chem.* C, 2007, **111**, 13763–13769.

41 Ö. A. Yıldırım, C. Durucan, *J. Alloys Compd*, 2010, **506**, 944–949.

42 M. Purica, E. Budianu, E. Rusu and R. Gavrila, *Thin Solid Films*, 2002, **404**, 485-488.

43 K. G. Chandrappa and T. V. Venkatesha, *Nano-Micro Lett.*, 2012, **4**, 14.

44 Z. L. Wang, *J. Phys. Condens. Matter.*, 2004, **16**, 829.

45 A. H. Moharram, S. A. Mansour, M. A. Hussein and M. Rashad, *J. Nanomat.*, 2014, 716210.

46 D. Ramimoghadam, M. Z. B. Hussein and Y. H. Taufiq-Yap, *Chem. Central J.*, 2013, 7, 136.

47 L. Guo, S. Yang, C. Yang, P. Yu, J. Wang and W. Ge, *Appl. Phys. Lett.*, 2000, **76**, 2901-2903.

48 J. Dupont, R. F. Souza and P. A. Z. Suarez, *Chem. Rev.*, 2002, **102**, 3667.

49 M. Freemantle, An introduction to ionic liquids, *RSC Publishing*, Cambridge, 2010.

50 N. Papageorgiou, Y. Athanassov, M. Armand, P. Bonhˆote, H. Pettersson, A. Azam and M. Gr¨atzel, *J. Electrochem. Soc.*, 1996, **143**, 3099.

51 R. Kawano, H. Matsui, C. Matsuyama, A. Sato, M. A. B. H. Susan, N. Tanabe and M. Watanabe, *J. Photochem. Photobiol.*, A, 2004, **164**, 87.

52 M. Doyle, S. K. Choi and G. Proulx, *J. Electrochem. Soc.*, 2000, **147**, 34.

53 A. Noda, M. A. B. H. Susan, K. Kudo, S. Mitsushima, K. Hayamizu and M. Watanabe, *J. Phys. Chem.* B, 2003, **107**, 4024.

54 M. A. B. H. Susan, A. Noda, S. Mitsushima and M. Watanabe, *Chem. Commun.*, 2003, 938.

55 W. Lu, A. G. Fadeev, B. Qi, E. Smela, B. R. Mattes, J. Ding, G. M. Spinks, J. Mazurkiewicz, D. Zhou, G. G. Wallace, D. R. MacFarlane, S. A. Forsyth and M. Forsyth, *Science*, 2002, **297**, 983.

56 M. A. B. H. Susan, T. Kaneko, A. Noda and M. Watanabe, *J. Am. Chem.* Soc., 2005, **127**, 4976.

57 M. A. B. H. Susan, S. Saha, S. Ahmed, F. Begum, M. M. Rahman and M. Y. A. Mollah, *Mater. Res. Innovations*, 2012, **16**, 345.

58 M. S. Miran, H. Kinoshita, T. Yasuda, M. A. B. H. Susan and M. Watanabe, *Phys. Chem. Chem. Phys*., 2012, **14**, 5178.

59 M. S. Miran, T. Yasuda, M. A. B. H. Susan, K. Dokko and M. Watanabe, *RSC Adv*., 2013, **3**, 4141.

60 S. Rabieh and M. Bagheri, *Mat. Lett*., 2014, **122**, 190–192.

61 O. Oprea, O. Ciocirlan, A. Badanoiu and E. Vasile, *Cent. Eur. J. Chem*., 2014, **12**, 749-756.

62 K. Qi, J. Yang, J. Fu, G. Wang, L. Zhu, G. Liua and W. Zheng, *Cryst. Eng. Comm.*, 2013, **15**, 6729-6735.

63 Z. He and P. Alexandridis, *Phys. Chem. Chem. Phys*, 2015, **35**, 20.

64 X. Duan, J. Ma, J. Lian and W. Zheng, *Cryst. Eng. Comm*., 2014, **16**, 2550.

65 A. Wittmar, D. Gautam, C. Schilling, U. Dorfler, W. Mayer-Zaika, M. Winterer and M. Ulbricht, *Nanopart Res*. 2014, **16**, 2341.

66 R. Gandhi, S. Gowri, J. Suresh and M. Sundrarajan, *J. Mater. Sci. Technol*., 2013, **29**, 533-538.

67 F. Jakuphanoglu, S. Ilican, M. Caglar and Y. Caglar, *J. Optoelec. Adv. Mat.*, 2007, **9**, 2180.

68 G. Voicu, O. Oprea, B. S. Vasile and E. Andronescu, *Dig. J. Nanomater. Bios.*, 2013, **8**, 667-675.

69 B. Cheng, E. T. Samulski, *Chem. Commun.*, 2004, **986**.

70 W.J. Li, E.W. Shi, W.Z. Zhong and Z.W. Yin, *J. Cryst. Growth*, 1999, **203**, 186-196.

71 M. Sabbaghan, A. S. Shahvelayati and S. E. Bashtani, Solid State Sci., 2012, **14**, 1191-1195.

72 M. Sabbaghan, J. Beheshtian and S. A. M. Mirsaeidi, *J. Ceram. Int*., 2013, **12**, 119.

73 M. Marium, M. M. Rahman, M. Y. A. Mollah and M. A. B. H. Susan, *RSC Adv*., 2015, **5**, 19907.

74 M. A. M. Moazzen, S. M. Borghei, F. Taleshi, *Appl.Nanosci.*, 2013,**3**, 295–302.

75 B. N. Joshi, H. Yoon, H. Y. Kim, J. H. Oh, T. Y. Seong, S.C. James and S. S. Yoon, *J. Electrochem. Soc.*, 2012, **159,** 8, H716-H721.

View Article Online
DOI: 10.1039/C6RA14955C

RSC Advances

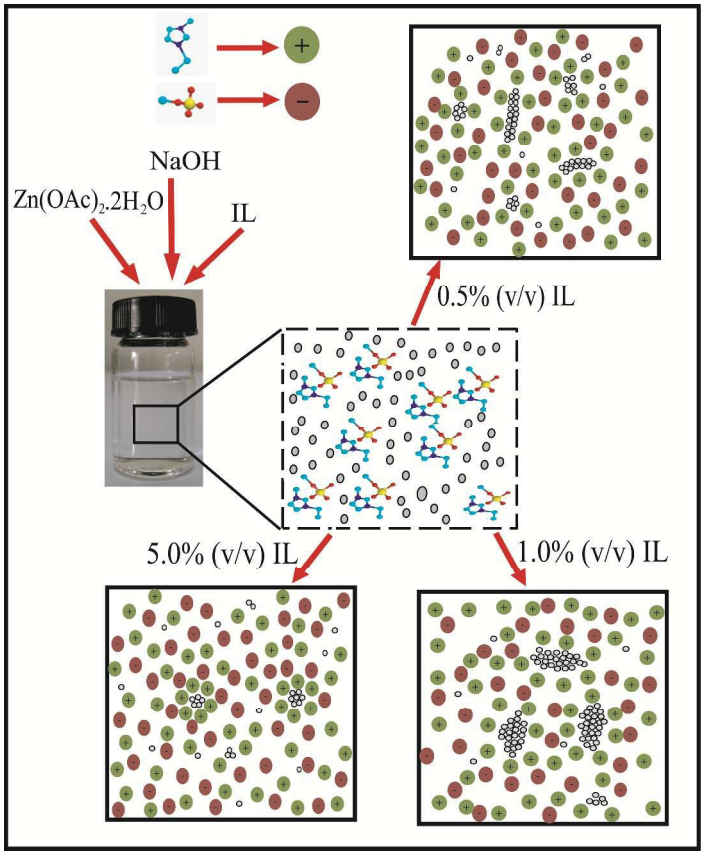

Hydrophilic ionic liquid-assisted control of size and morphology of ZnO nanoparticles prepared by chemical precipitation method†

Mousumi Akter, Shazia Sharmin Satter, Ajaya Kumar Singh, M. Muhibur Rahman, M. Yousuf A. Mollah, and Md. Abu Bin Hasan Susan

A hydrophilic ionic liquid (IL), [EMIM][$MeSO_4$] served as a self directing template during synthesis of ZnO nanoparticles by chemical precipitation method and the size, shape and morphology of ZnO nanoparticles depended on the concentration of the IL due to hydrogen-bonding and π-π* interaction between the IL and ZnO nanoparticles.